Seasonal mixed-layer salinity balance in the tropical Atlantic Ocean: Mean state and seasonal cycle

Casimir Da-Allada, Gaël Alory, Yves Du Penhoat, Elodie Kestenare, Fabien Durand, Norbert Hounkonnou

JOURNAL OF GEOPHYSICAL RESEARCH: OCEANS, VOL. 118, 332–345, doi:10.1029/2012JC008357, 2013

Seasonal mixed-layer salinity balance in the tropical Atlantic Ocean: Mean state and seasonal cycle

C. Y. Da-Allada,[1,2,3] G. Alory,[1,5] Y. du Penhoat,[2,3,4] E. Kestenare,[1,3] F. Durand,[1,3] and N. M. Hounkonnou[2]

Received 13 July 2012; revised 29 November 2012; accepted 2 December 2012; published 30 January 2013.

[1] We investigate the causes of the seasonal cycle of the near-surface salinity using a mixed-layer salinity model and a combination of satellite products, atmospheric reanalyses, and in situ observations for the period 2000–2008, in the tropical Atlantic Ocean. We find that the balance differs from one region to another. In the western tropical Atlantic, it is controlled by horizontal advection from March to November and by freshwater flux and entrainment for the rest of the year. In the central tropical Atlantic, it is mainly due to the strong contribution of precipitation in agreement with previous results. In the northeastern tropical Atlantic, all terms contribute to the mixed layer salinity between December and March; during the rest of the year, precipitation and zonal advection mainly control the balance. In the Gulf of Guinea, it is driven by freshwater flux from October to February; from March to July, it is controlled by horizontal advection and entrainment; from August to September, mixed-layer salinity variability is weak. Finally, in the Congo region, it is driven by freshwater flux (precipitation and runoff from Congo River) from September to December, by horizontal advection during January to March, and by vertical entrainment during the rest of the year (April to August). There are some discrepancies between observed and modeled salinity tendencies. Some of them are due to our model formulation, which does not explicitly account for the effect of vertical diffusion. Uncertainties of observation products, which force the model, are also sources of errors.

Citation: Da-Allada, C. Y., G. Alory, Y. du Penhoat, E. Kestenare, F. Durand, and N. M. Hounkonnou (2013), Seasonal mixed-layer salinity balance in the tropical Atlantic Ocean: Mean state and seasonal cycle, *J. Geophys. Res. Oceans*, *118*, 332–345, doi:10.1029/2012JC008357.

1. Introduction

[2] The tropical Atlantic Ocean is characterized by strong seasonal river discharge with the Amazon and Congo Rivers accounting for around 20% of the world river discharges. This creates regions of low sea surface salinity (SSS) off these major rivers. In addition, strong precipitations in the Intertropical Convergence Zone (ITCZ) also lead to a region of low SSS around 5°N. In contrast, SSS exhibits high values in the North and South subtropical gyres where evaporation associated with winds dominates over precipitation.

[3] Salinity can have an important role on ocean circulation due to its contribution to buoyancy and stratification of the water column. Specifically, it can affect the exchange of heat between the warm surface layer and the colder lower layers of the tropical ocean, and consequently between the upper ocean and the atmosphere [*Lukas and Lindstrom*, 1991; *Sprintall and Tomczak*, 1992]. From observations, *Pailler et al*. [1999] showed that this effect is important in the tropical western Atlantic basin. *de Boyer Montégut et al*. [2007] and *Mignot et al*. [2007] noted the presence of quasi-permanent barrier layers in the north western tropical Atlantic, using a climatology of differences between temperature and salinity stratification. It also seems that occurrences of barrier layer have been observed at times in the eastern part of the basin (Bourlès and Guivarc'h, personal communication, 2003). SSS could also be the best indicator of freshwater flux to the ocean surface as suggested by *Yu* [2011]. The study of SSS is therefore crucial for our understanding of the internal dynamics of the ocean and for climate studies [*Lagerloef*, 2002].

[4] The key role of SSS in the climate system has motivated a number of studies both from observations and models, aiming at describing and understanding the physical processes responsible for SSS variations in the tropical ocean. *Johnson et al*. [2002] used a combination of climatological SSS and satellite-derived surface currents to estimate the horizontal divergence of SSS in the global tropics in a mean and at seasonal time scale. They found the seasonal divergence to represent a significant fraction of the annual

[1]Université de Toulouse, UPS (OMP), LEGOS, Toulouse, France.
[2]ICPMA, Université d'Abomey-Calavi, Cotonou, Bénin.
[3]IRD, LEGOS, Toulouse, France.
[4]IRD, CRHOB, Cotonou, Bénin.
[5]CNAP, LEGOS, Toulouse, France.

Corresponding author: C. Y. Da-Allada, Université de Toulouse, UPS (OMP), LEGOS, 14 Av. Edouard Belin, F-31400 Toulouse, France. (daallada@yahoo.fr)

2169-9275/13/2012JC008357

mean divergence. *Dessier and Donguy* [1994] investigated the causes of SSS variations in the tropical Atlantic measured from voluntary observing ships (VOS) and research vessels. They found a pronounced seasonal cycle of SSS throughout most of the basin. They concluded that SSS variability is mainly controlled by precipitation due to the ITCZ in the east of the basin, while it is mainly governed by freshwater outflow from the Amazon and Orinoco rivers in the west of the basin. However, their study was limited by data availability and they did not explicitly estimate the contributions from horizontal or vertical salinity advection. *Delcroix et al*. [2005] with an extended data set based on VOS tracks, TAO/TRITON, and Pilot Research Moored Array in the Tropical Atlantic (PIRATA) moorings, determined the characteristic time and space scales of SSS variations in the three tropical oceans. *Reverdin et al*. [2007] extended previous studies in the tropical Atlantic by mapping monthly SSS with observations collected from 1977 to 2002 to extract the large-scale variability. They found that seasonal SSS variability is maximum in the regions of the ITCZ, the North Equatorial Countercurrent (NECC), off the northern part of South America and in the eastern Gulf of Guinea. Using observations at four PIRATA moorings located at 15°N, 12°N, 8°N, and 4°N along 38°W, *Foltz et al*. [2004] examined the seasonal mixed-layer salinity (MLS) balance and showed that it is due to a large extent to seasonal variations in horizontal salinity advection and precipitation along this meridian. This study was extended to the northern part of the tropical Atlantic by *Foltz and McPhaden* [2008] using a combination of satellite products, in situ observations, and atmospheric reanalyses. They found that the contributions to the salinity balance varied from a region to another. In the western tropical North Atlantic, horizontal salinity advection was the dominant process. In the north-central basin, a very weak seasonal cycle of MLS was mainly due to a balance between meridional advection and an excess of evaporation over precipitation. Farther south, they found that the seasonal cycle of MLS was mainly influenced by seasonal variations in precipitation. However, the contribution of entrainment term and diffusion term was not explicitly estimated by the authors. Both processes were included in a residual term.

[5] Most of these studies on SSS are limited by the lack of in situ measurements and they do not explicitly take into account all terms of the MLS balance. Recently, the density of available observations in salinity has greatly increased in the Atlantic Ocean thanks to Argo data (http://www.coriolis.eu.org/Observing-the-ocean/Observing-system-networks/Argo). Argo profiling floats provide salinity measurements with good spatial and temporal coverage (with typically one profile every 300 km and every 10 days). Therefore, they could help to answer the following remaining questions on SSS in the tropical Atlantic Ocean: Is it possible to estimate the salinity variability from the available data (precipitation, evaporation, runoffs from rivers, horizontal oceanic transport)? If so, at which time and space scale is this possible? Which variable (evaporation, precipitation, or horizontal currents) is the MLS balance the most sensitive to? What are the mechanisms responsible for the salinity variability in the mixed layer in the tropical Atlantic Ocean? In particular what is the contribution of each term of the MLS balance to the seasonal cycle?

[6] To address these questions, we use in this study a new in situ gridded SSS product for the Atlantic Ocean covering the Argo period, and we develop an MLS model to diagnose seasonal SSS variations from available observations of freshwater fluxes, oceanic currents, and mixed layer depth. This model allows exploring the various processes involved in the seasonal SSS budget and the sensitivity of the later to the various forcing variables.

[7] The remainder of this paper is organized as follows. Section 2 describes the model and the data sets used in the study. Section 3 presents the results, including MLS model validation and sensitivity to the observed forcing, mean and seasonal MLS. Section 4 provides a summary and discussion of the most important results.

2. Model and Data

2.1. Model

[8] Following *Foltz et al*. [2004], we assume that MLS is very close to SSS. Therefore simulated MLS is compared to observed SSS to evaluate the model skill. Our study is based on a bi-dimensional model of MLS implemented on our study area, the tropical Atlantic basin (20°N–20°S, 60°W–20°E). This model relies on a spatial and temporal discretization of the salinity evolution equation in the mixed layer:

$$\frac{\partial S_m}{\partial t} = \frac{(E-P-R)S_m}{h_m} - \overrightarrow{u_m}.\vec{\nabla}S_m - H(w_e)\frac{(S_m - S_{h_m})}{h_m} + K\nabla^2 S_m \tag{1}$$

where S_m is the MLS, t is time, E-P-R is the surface freshwater flux including evaporation (E), precipitation (P), and river runoff (R), h_m is the mixed layer depth (MLD), $\boldsymbol{u_m}$ is the horizontal velocity, S_{h_m} is the salinity just below the mixed layer, $w_e = w + \frac{\partial h_m}{\partial t}$ is the entrainment velocity (at depth $z = -h_m$) which corresponds to the difference between the vertical velocity w (positive when upward) at the mixed-layer base and the mixed-layer deepening rate, $H(w_e)$ is the Heaviside step function ($H(w_e) = w_e$ if $w_e > 0$; $H(w_e) = 0$ if $w_e < 0$), and K is the horizontal diffusivity.

[9] The varying thickness of the mixed layer is used to approximate the vertical physics in the form of the entrainment term. The vertical processes at the base of the mixed layer are taken into account by means of the entrainment velocity (estimated from the horizontal currents through the continuity equation) only in case of thickening of the mixed layer (situation of entrainment), then the deep water will mix with water from the surface layer and therefore will modify its properties. When the mixed-layer shoals (detrainment situation), the entrainment velocity is thus set to zero.

[10] Equation (1) is similar to that used in other salinity studies [e.g., *Delcroix and Hénin*, 1991; *Rao and Sivakumar*, 2003; *Dong et al*., 2009]. S_m is the only freely evolving variable in the model while all other variables are prescribed from observations.

[11] The model grid is set to 1° in latitude and longitude which is the spatial resolution commonly available for observations. The time step is set to 1 day to ensure numerical stability given the spatial resolution and maximum horizontal velocities. We record monthly outputs which are sufficient to identify the dominant processes driving the seasonal

evolution of MLS. We use in our model the Arakawa C grid allowing a decentered discretization. The mask of the model depends on these variables and corresponds to the largest oceanic domain common to all prescribed observations. It is primarily restricted by the spatial coverage of the current product. The zonal velocity is set to zero at western and eastern continental boundaries, and the meridional velocity is set to zero at the northern and southern continental boundaries. At the ocean boundaries (20°N, 20°S, 60°W), observed salinities are imposed in order to calculate realistic horizontal salinity gradients.

[12] We only considered the three most important rivers (Amazon, Congo, and Niger) in our study area. We used the runoff data of *Dai et al*. [2009]. We spread the outflow of each river over four model grid points off the mouth, as the model mask does not extend to the coastline. We made several tests to place these river runoffs, which revealed that our model is very sensitive to their location. We have not explicitly taken into account the Orinoco River: the 60°W western limit of our domain of study is located to the east of the estuary to exclude the complex topography of the Caribbean Sea which cannot be resolved at the model resolution. However, we prescribe observations of SSS at this ocean boundary to account for it.

[13] We also assume that the lateral diffusion is constant in the mixed layer, as *Dong et al*. [2009]. K is then set to the average value found in the literature, $2000\,m^2\,s^{-1}$, throughout the basin [e.g., *Kawabe*, 2008]. Sensitivity tests show that the background value of K does not influence the results. However, we set this value to $7000\,m^2\,s^{-1}$ on the river grid points to account for the large sub-grid scale mixing in these estuary regions. We justify this procedure by the fact that we do not resolve near-coastal dynamics.

[14] To run the model, initial conditions in MLS are set everywhere to a constant value of 35, roughly the mean value of ocean salinity. Then we let the model freely evolve under the influence of observed forcing and simulated processes. Whatever the observed products used as forcing, the model converges to a stable and repeated seasonal cycle after a spin-up period of about 2 years. The simulated seasonal cycle of MLS in year 3 is therefore used as the model reference. Various global fields of near-surface currents and surface freshwater fluxes are available. The model is a suitable tool to test their ability to close the MLS budget when combined together.

2.2. Data

[15] As explained in the previous section, several variables are needed to force and to assess the MLS model: freshwater flux, currents, MLD, and surface and subsurface salinity. The various data sources are described below. If not already available in this format, data are sub-sampled or interpolated on a 1° grid and a monthly climatology is computed from each dataset for the 2000–2008 period that is commonly available.

2.2.1. Net Freshwater Flux

[16] The net freshwater flux, E-P-R, includes three components: evaporation (E), precipitation (P), and runoffs (R). For E and P, data are obtained from atmospheric reanalyses and satellite data sets. We use ERA-Interim reanalysis [*Dee et al*., 2011] from the European Centre for Medium-Range Weather Forecasts (ECMWF) and NCEP2 reanalysis [*Kanamitsu et al*., 2002] from the National Centers for Environmental Prediction (NCEP). Both data sets are available monthly at 1.5° resolution for ERA-Interim and at 2° resolution for NCEP2. We also use E from the Objectively Analyzed air-sea Fluxes (OAFlux) data set [*Yu et al*., 2008] which is a monthly value at 1° resolution. Finally, we also consider three observed P products issued from Global Precipitation Climatology Project (GPCP) [*Adler et al*., 2003], Climate Prediction Center's Merged Analysis of Precipitation (CMAP), and enhanced CMAP (CMAPE) [*Xie and Arkin*, 1997]. Both CMAP and GPCP combine measurements from rain gauges and from satellite infrared and microwave sensors. They are available on a 2.5° grid. In CMAPE, the CMAP data set is complemented with precipitation values from NCEP reanalysis. For R, we considered the *Dai et al*. [2009] product which gives climatological runoff for major world rivers at their estuary. In the tropical Atlantic, it includes 32 rivers, the main ones being the Amazon, Congo, Orinoco (actually the three largest river flows in the world), and Niger. Amazon, Congo, and Niger Rivers bring 211,000, 41,000, and $6000\,m^3\,s^{-1}$, respectively, on yearly average, which represents 85% of the total runoff in our oceanic domain.

2.2.2. Surface Currents

[17] Surface currents were obtained from three different sources to estimate horizontal mixed layer velocity. The Ocean Surface Current Analysis Realtime (OSCAR) currents are estimated from satellite sea level, wind stress, and SST, together with a diagnostic model [*Lagerloef et al*., 1999]. OSCAR horizontal velocity includes both geostrophic and Ekman components and represents the mean current between the surface and 30 m depth [*Bonjean and Lagerloef*, 2002]. They are representative of currents at an average of 15 m depth. We select the filtered OSCAR product available on a $1° \times 1° \times 5$ day grid (note that a 1/3° product is also available). For validation and error analysis of OSCAR, see *Johnson et al*. [2007]. The currents from Centre de Topographie des Océans et de l'Hydrosphère (CTOH) are computed in the same way as OSCAR currents but have a 1/4° spatial resolution and are available weekly [*Sudre and Morrow*, 2008]. Finally, we use near-surface velocity from satellite-tracked drifting buoy observations (henceforth DRIFTER product), which are available on a monthly mean climatology on a $1° \times 1°$ grid [*Lumpkin and Garzoli*, 2005]. Compared to satellite-derived currents, drifter currents are available closer to the coast. Drogue-loss problems have been recently identified for some drifters [*Grodsky et al*, 2011]. However, using a preliminary corrected version of the product in our model did not significantly change the model's skills.

2.2.3. Subsurface Data

[18] Mixed layer depth (MLD) is taken from the climatology of *de Boyer Montégut et al*. [2004], available monthly on a $2° \times 2°$ grid. It is estimated from individual temperature and salinity profiles extracted from National Oceanographic Data Center (NODC) and World Ocean Circulation Experiment (WOCE) data. We use the mixed layer depth based on a density criterion ($0.03\,kg\,m^{-3}$) so that both temperature and salinity stratifications are taken into account.

[19] Subsurface salinity data originate from the 2009 World Ocean Atlas (WOA09). They are provided as a monthly

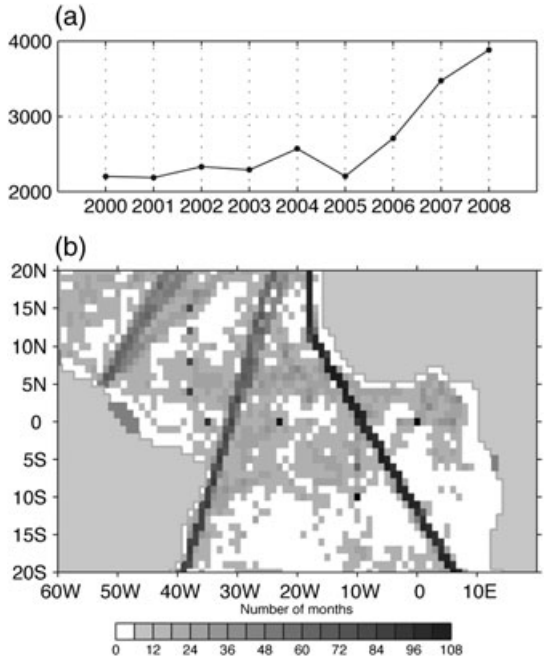

Figure 1. (a) Sea surface salinity data distribution indicating the number of $1° \times 1°$ grid points with data in a month as a function of year. (b) The spatial distribution of the number of months with data in $1° \times 1°$ box for 2002–2008.

climatology on a $1° \times 1°$ grid and were constructed using all types of available observations [*Boyer et al*., 2009]. The climatology of salinity below the mixed layer (S_{h_m}) is constructed from this field, by extracting for each month and each grid point, the salinity vertically interpolated at the mixed layer depth. Salinity values are given in the Practical Salinity Scale (PSS-78) and reported without units as recommended [*Millero*, 1993].

2.2.4. Sea Surface Salinity

[20] The observed SSS fields developed by *Reverdin et al*. [2007] have been recently extended to 2009 (see http://www.legos.obs-mip.fr/kestenare). As given by *Reverdin et al*. [2007], the monthly SSS is gridded using an objective mapping [*Bretherton et al*., 1976] at $1° \times 1°$ spatial resolution, by compiling a variety of data sources, mostly from underway thermosalinographs on research vessels and voluntary observing ships (http://www.legos.obs-mip.fr/observations/sss/), from PIRATA moorings in the tropical Atlantic (http://www.brest.ird.fr/pirata/), from SMOS and CARIOCA drifters [G. Reverdin, personal communication], and from Argo floats (http://www.coriolis.eu.org/Observing-the-ocean/Observing-system-networks/Argo). Figure 1a shows the temporal evolution of the available data (before objective analysis) which increased considerably after 2005 by including the Argo floats. Similarly, Figure 1b shows a map of the overall data density which presents a marked spatial contrast: some areas show a poor data coverage (as the southern Atlantic and the south-east of the basin) while large density areas are seen along the repeated cargo lines. We chose this product as a reference for model evaluation as it is, to our knowledge, the most complete and up-to-date product for SSS available, especially dedicated to the surface layer and to the Atlantic basin.

[21] We focused on the 2000–2008 period to build the mean seasonal cycle of SSS. We retained only the grid points where the estimated RMS error (normalized by the signal amplitude) does not exceed 0.8, as by *Reverdin et al*. [2007], and so we excluded the grid points where observations are too sparse.

3. Results

[22] The observed mean SSS field is presented in Figure 2. It presents high values of SSS in the northern (around 15°N) and southern (around 15°S) subtropical gyres due to intense evaporation in these regions. Regions of low SSS are located under the ITCZ region due to strong precipitation. SSS minimum values are observed near the continents due to strong river discharges into ocean (off the Amazon, Congo, and Niger Rivers in particular). The regions of large SSS variability are found near the mouths of these rivers and in the ITCZ along 8°N (Figure 2b).

3.1. Sensitivity of the Model to the Various Forcing Variables

[23] As by *Foltz and McPhaden* [2008], we focus on different regions of the tropical Atlantic Ocean where MLS variability is large. Based on the standard deviation of SSS (Figure 2b), we select five regions: the western tropical Atlantic (WTA), the central tropical Atlantic (CTA), the eastern tropical Atlantic (ETA), the Gulf of Guinea region (GG), and the Congo region (CO). To study the seasonal cycle of the MLS, we need first to tune the model so that the simulated MLS is as close as possible to the observed MLS. Surface currents and net freshwater flux (E-P) are available from different sources. We test the sensitivity of the model to these different products in the whole tropical Atlantic and in the selected regions.

[24] For the freshwater flux (E-P), five monthly climatology products were tested. In addition to NCEP2 and ERA-Interim monthly climatology which directly provides E-P, we constructed three other monthly climatological products combining different sources, namely E (OAFlux)-P (CMAP), E (OAFlux)-P (CMAPE), and E (OAFlux)-P (GPCP). ERA-Interim and NCEP2 freshwater fluxes are shown in Figure 3 and give the lower and upper ranges of observations, respectively. In both products, evaporation is maximum around 15°N and 15°S, while precipitation is maximum around 5°N due to the ITCZ and weakens on either side of the ITCZ area (Figure 3).

[25] The three surface currents tested are presented in Figure 4. All products show the main components of the tropical current system: the westward South and North Equatorial Currents (SEC/NEC) around the equator and 15°N, respectively, the eastward North Equatorial Counter Current (NECC) around 10°N, the northwestward coastal North Brazil Current (NBC) between 5°S and 10°N, and the eastward Guinea Current (GC) along the northern coast of the Gulf of Guinea. However, there are marked differences in current patterns in the 5°N–5°S equatorial band, in direction as well as in magnitude. The weakest currents are found in the OSCAR product and the strongest in the DRIFTER product. An equatorial divergence is seen in the latter only. The DRIFTER product also extends closer to the coast than the other products, revealing a particularly

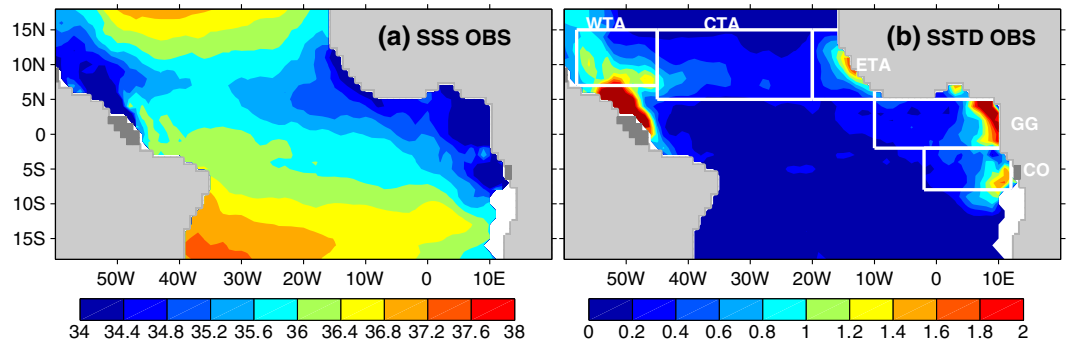

Figure 2. (a) Annual mean and (b) seasonal standard deviation for SSS observations. Sub-regions used in the study are marked.

strong western boundary NBC. However, to compare the effect of different currents in the model, we used a common mask (corresponding to OSCAR current mask) by removing part of the coastal currents in the DRIFTER product.

[26] To evaluate the model sensitivity to forcing variables, all combinations of the above freshwater and current products were tested and used as model forcing. For each of these combinations, the 12 modeled monthly SSS maps were visually compared to the 12 observed climatological maps. In addition to basin-scale maps, regional maps were also compared. We quantified the similarity between the modeled and observed sets of maps by computing the statistical parameters that are summarized in the Taylor diagrams [*Taylor*, 2001] shown in Figure 5, for the whole basin and two representative sub-regions. On these diagrams, the difference in skills between model versions is primarily due to current products, while different freshwater flux products create smaller differences in skills. This is particularly obvious in the GG region. Therefore, the model appears more sensitive to currents than to freshwater flux. OSCAR and CTOH currents give relatively similar results while the model consistently performs better with DRIFTER currents. Among the various freshwater flux products, NCEP2 gives the poorest skills in the whole basin and in most regions. Other fluxes give roughly similar results although ERA-Interim often slightly improves skills. We choose this flux because it gives in most regions the best correlation and the best (closest to 1) standard deviation ratio. Based on these statistics, the DRIFTER currents and ERA-Interim freshwater flux appear as the most appropriate forcing products for the SSS budget. We therefore use this set of products to force the model in the rest of this study. Moreover, we henceforth use the DRIFTER current mask. Coastal currents are then fully accounted for and model skills are again improved, particularly in the WTA region (Figure 5b).

3.2. Mixed-Layer Salinity Model Validation

[27] The above sensitivity study allowed identifying the most appropriate forcing strategy for the model. Now, in this optimal configuration, the model outputs can be directly compared to observations. The model mean and seasonal STD of SSS shown in Figures 6a and 6b can be compared to the equivalent maps based on observations (Figure 2). For the mean state (Figure 6a), the model reproduces the

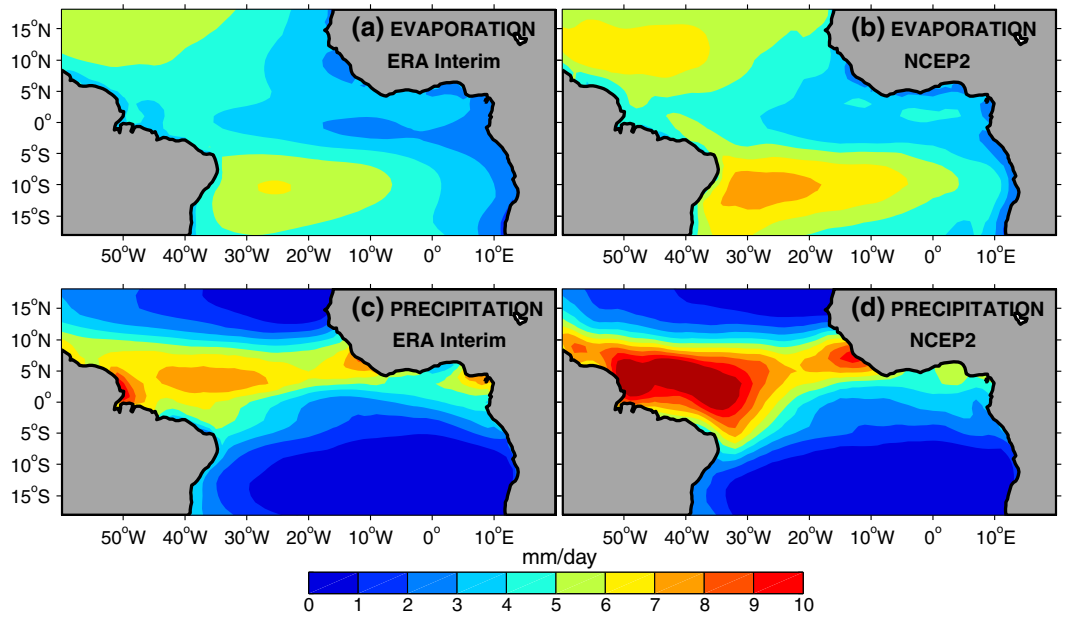

Figure 3. Annual mean for evaporation products, (a) ERA-Interim and (b) NCEP2, and for precipitation products, (c) ERA Interim and (d) NCEP2. Units are mm day^{-1}.

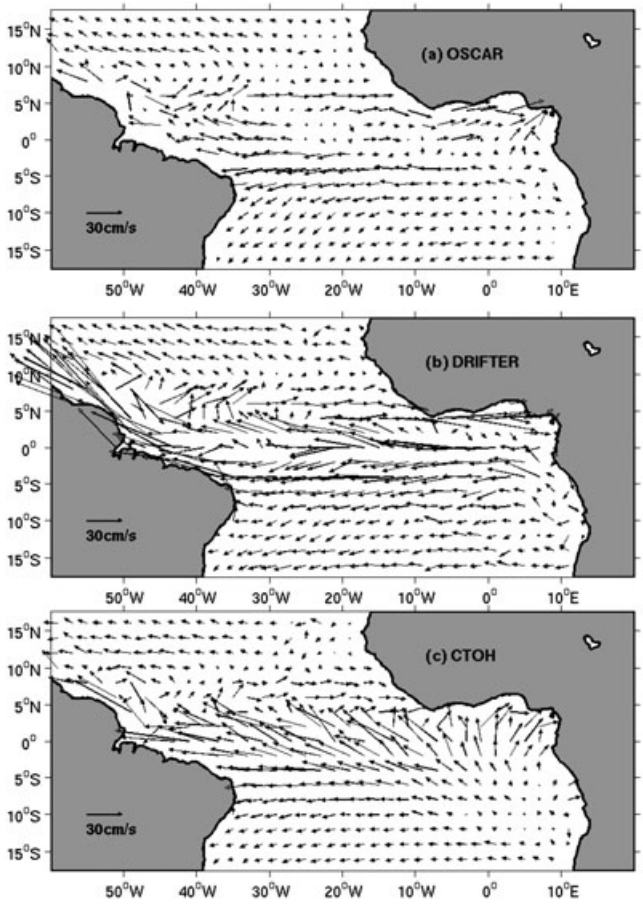

Figure 4. Annual mean for surface currents products (a) OSCAR, (b) DRIFTER, and (c) CTOH. Units are cm s^{-1}.

high salinity observed (Figure 2a) in the northern and southern subtropical gyres due to the intense evaporation in these regions. However, the modeled SSS is slightly lower than observed in the southern subtropical gyre (15°–20°S, 30°–40°W). This could come from the representation of the freshwater flux. The model also shows areas of low salinity due to the ITCZ or related to river runoffs (Amazon, Congo, and Niger) as observed in this basin. Note however that the modeled SSS is slightly lower than observed in the central part of the ITCZ (5°–10°N, 20°–45°W). On the contrary, it is slightly higher than observed in the northwest of the basin (5°–15°N, 50°–60°W). This could be explained by an incorrect redistribution of Amazon waters between the coastal NBC and its eastern retroflection feeding the NECC (Figure 7) [*Bourlès et al*., 1999].

[28] The SSS standard deviation (SSTD) of the model (Figure 6b) shows areas of large seasonal variability, mostly properly located as compared to observations (Figure 2b): near the mouths of the rivers (Amazon, Congo, and Niger) and in the 5°–10°N latitude band due to the meridional displacement of the ITCZ. However, the observed SSTD always shows larger variability than the model at river mouths. This may be due to minor rivers not accounted for, which cumulative contribution may not be negligible, and/or to fine-scale processes unresolved by the model (such as vertical diffusion). Also, note that observed high coastal SSS variability is not necessarily associated with rivers only and can be due to an amplification of the seasonal cycle of precipitation around coastal mountains (e.g., Fouta Jallon near 10°N, 15°W, or Mount Cameroon near 5°N, 10°E close to the Niger mouth). In the model there are two patches of larger than observed SSS variability near 3°N and 5°S extending westward from the coast of Africa, which could be due to an overestimation of the two westward branches of the SEC (Figure 7a) located on each side of the equator in the current product we use.

3.3. Mean Salinity Balance in Atlantic Ocean Basin

[29] The model quickly converges to a stable seasonal cycle of SSS indicating that, on annual mean, the oceanic processes (advection, diffusion, and entrainment) are balanced by the contributions of the freshwater flux E-P-R (Figure 8). This is expected in nature. However, to achieve that in the model, the entrainment term is very helpful. While this term has a physical formulation, it also tends to damp the model SSS toward the prescribed climatology of salinity below the mixed layer, which makes it essential for the stability of the model. This damping effect is illustrated in Figures 6c and 6d: the vertical salinity gradient is roughly anticorrelated to the model error, which helps correcting the model when entrainment is at work. Entrainment also tends to be anticorrelated with horizontal advection, at small scale (Figure 8), which is probably real. These small-scale features originate from the 1° resolution drifter currents. As vertical velocity (which dominates entrainment velocity) is calculated from the horizontal currents by mass continuity, and both horizontal and vertical velocity are multiplied by salinity gradients involving locally the same SSS to compute advection and entrainment, respectively, it is expected that advection and entrainment have similar small-scale features, but with opposite sign. On the other hand, the fact that entrainment damps the model toward climatology probably helps to smooth the sum of oceanic processes, which reflects the smoothness of the freshwater flux, due to its 2.5° original resolution.

[30] The net freshwater flux (Figure 8c) is negative mainly from the equator to 10°N and also near the mouth of the Congo, which corresponds to a net intake of freshwater for the ocean and causes a freshening of the mixed layer. This is due to the strong precipitations in the ITCZ and to river runoffs. Over the rest of the Atlantic Ocean basin, this term shows positive values as it is dominated by evaporation and therefore tends to increase the salinity. As shown in Figure 8d, the contributions of oceanic processes and freshwater flux are similar but with opposite signs.

[31] By splitting the oceanic processes into horizontal advection, horizontal diffusion, and vertical entrainment terms, we note that the horizontal diffusion term is negligible except near the mouths of rivers where there are strong SSS gradients. Therefore, we only show the advection and entrainment terms in Figures 8a and 8b. To further explore the processes, we decompose horizontal advection into zonal and meridional terms (Figure 9) and plot zonal and meridional SSS gradients (Figure 10). Roughly, in the open ocean advection tends to decrease SSS north of 10°N and south of 2°N, while it tends to increase SSS between 2°N and 10°N. The picture is more complex in the coastal areas.

[32] North of 10°N, the zonal SSS gradient is positive in the western half of the basin and negative in the eastern half

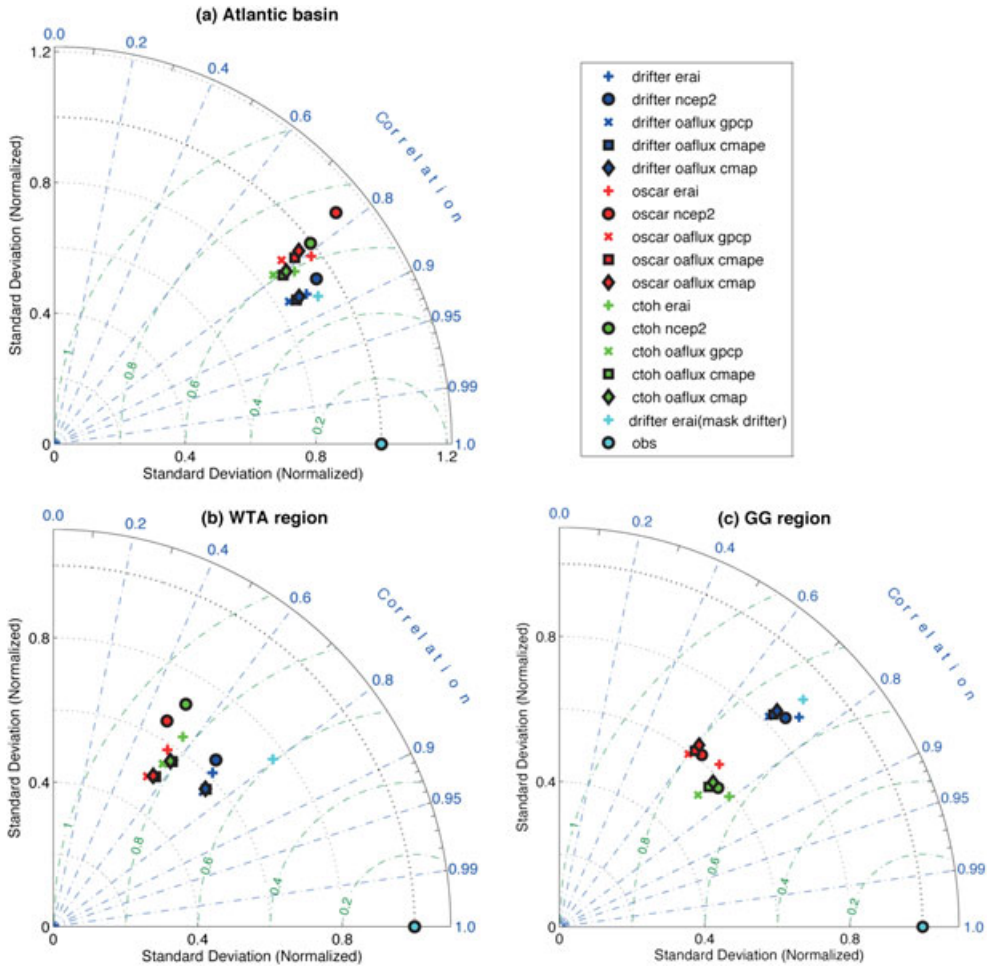

Figure 5. Taylor diagrams. Observations and model are represented by points on a diagram where the spatial correlation coefficient (R) between the observed and modeled maps is given by the azimuthal position, spatial standard deviation of the observed or modeled map is given by the radial distance from the origin, and the spatial centered root mean square difference (RMSD) is given by the distance between the observed points and model point (a) in the whole domain, (b) in the WTA box, and (c) in the GG box.

(Figure 10a), as SSS decreases toward the coast (Figure 6a). Zonal advection by the westward NEC (Figure 7a) therefore tends to increase SSS in the western half and decrease it in the eastern half (Figure 9a). The meridional SSS gradient is positive as SSS increases northward of the SSS minimum in the ITCZ (Figure 10b) and the meridional flow is northward (Figure 7b). Meridional advection therefore tends to decrease SSS (Figure 9b). Meridional advection dominates over zonal advection in the western half while both cumulate in the eastern half, which results in the negative advection tendency north of 10°N.

[33] Between 2°N and 10°N, the zonal SSS gradient is again positive in the west and negative in the east (Figure 10a) but currents are largely eastward here, dominated by the NECC and GC (Figure 7a). Therefore, zonal advection tends to decrease SSS in the western half and to increase it in the eastern half (Figure 9a). Meridional advection is relatively small in the east. In the west, the meridional SSS gradient is negative as the ITCZ-related SSS minimum is located further north (Figure 9b), and the strong meridional flow is northward due to equatorial divergence (Figure 7b). Meridional advection is therefore positive and dominates over zonal advection there. This results in a positive advection tendency in this latitude band.

[34] South of 2°N, the zonal SSS gradient is negative due to the Niger and Congo outflows in the east (Figure 10a). The zonal flow is dominated by the westward SEC with its two branches on each side of the equator (Figure 7a), resulting in a negative zonal advection tendency. The meridional SSS gradient is mostly negative in this transition zone between the wet tropics and dry subtropics (Figure 10b), and the meridional flow is southward to the south of the equator (Figure 7b), resulting in a negative meridional advection tendency. Overall, this results in a negative advection tendency to the south of 2°N, particularly strong along the path of the SEC.

[35] North of the equator along the South American coast and south of the equator along the African coast, river runoffs create strong small-scale SSS gradients (Figure 10). In addition to large-scale zonal flows, there are strong alongshore currents: the northwestward NBC and its retroflection at the western boundary, the southward coastal Angola current, and the northward Benguela current extension (further offshore) at the eastern boundary (Figure 7). As a result,

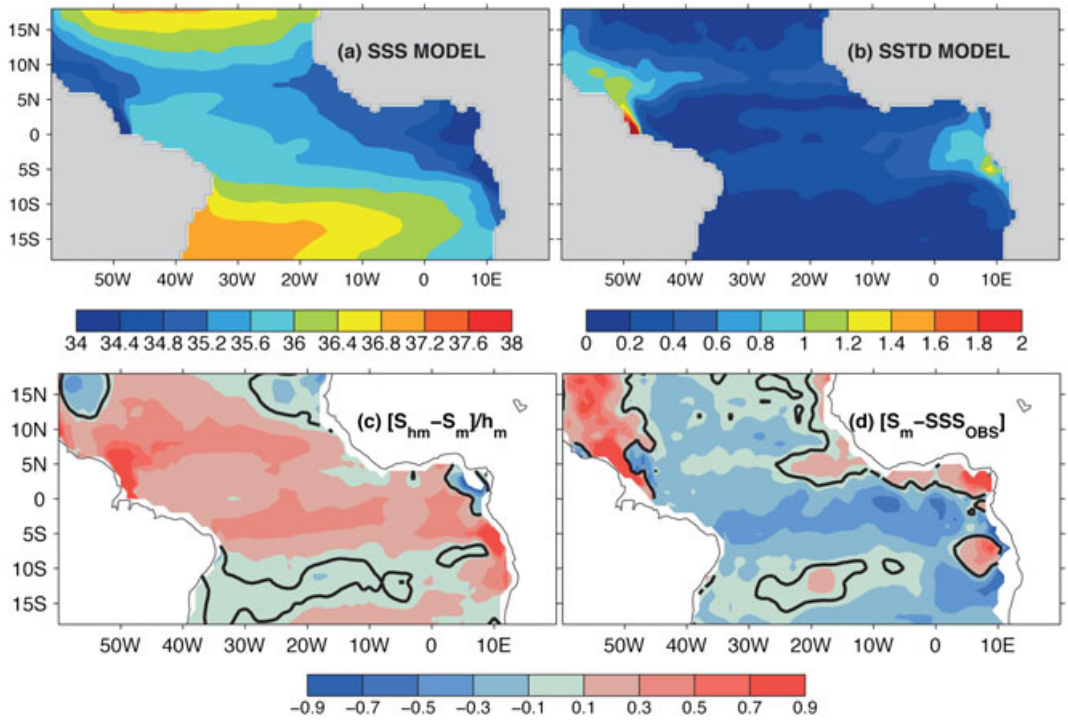

Figure 6. Annual mean for (a) SSS model, (b) seasonal standard deviation for SSS model, (c) $(S_{hm} - S_m)/h_m$, and (d) salinity difference between the model and observations in the tropical Atlantic Ocean. Heavy contours are the zero line.

zonal and meridional advections compete with each other (Figure 9) and the total advection is particularly strong, highly heterogeneous with alternating positive and negative patches.

[36] The entrainment term (Figure 8b) is positive and therefore tends to increase MLS over most part of the basin. It is particularly strong along the equator, along 10°N and in the Amazon and Congo plumes. As entrainment corresponds to an inflow of subsurface water into the mixed layer, its positive sign is explained by the saltier waters generally found just below the mixed layer (Figure 6c). This vertical salinity gradient is particularly strong in regions of low SSS, which explains the strong contribution of entrainment along 10°N and in the Amazon and Congo plumes. Along the equator, the strong entrainment term is due to the equatorial upwelling (driven by Ekman divergence). This brings into the mixed layer saltier waters from the Equatorial Undercurrent [*Bourlès et al.*, 2002] and from the North and South Equatorial Undercurrents (NEUC around 4°N, and SEUC around 3°S); all these limbs originate from the subtropical regions of high evaporation. The few regions where the entrainment term is negative (off the Niger mouth, in the north-west and north-east corners of the model domain, along 10°–15°S) are regions where the model overestimates SSS (Figures 6c and 6d). Thus, subsurface waters appear to be less salty than the MLS which is probably spurious. This is particularly true off the Niger mouth. Also, in the north-west region, as already suggested above, this is probably due to the coastal NBC that does not advect enough Amazon freshwaters in that region. Therefore, these waters

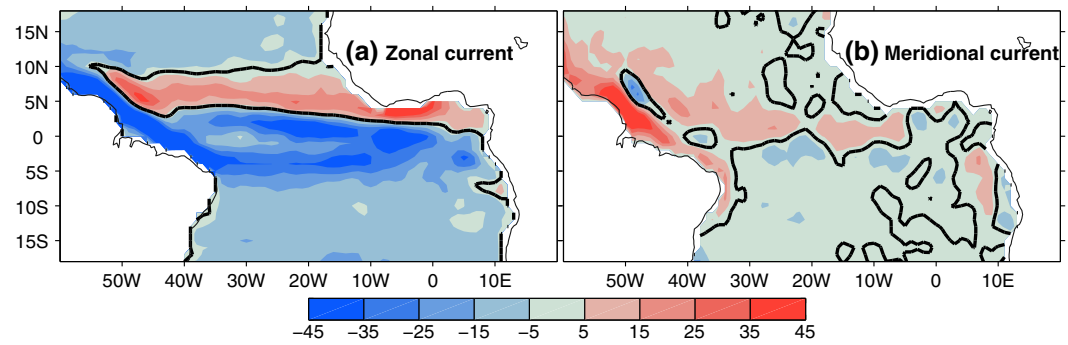

Figure 7. Annual mean for the (a) zonal and (b) meridional DRIFTER surface currents. Heavy contours are the zero line. Units are cm s^{-1}.

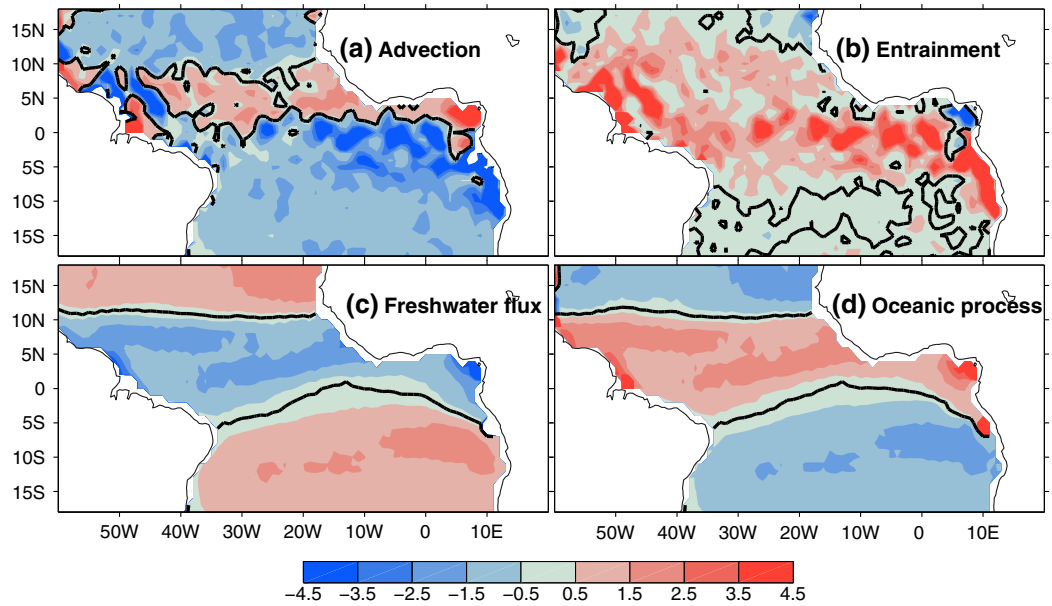

Figure 8. Annual mean for the salinity balance terms (in yr^{-1}) from the simulation: (a) horizontal advection, (b) entrainment, (c) surface freshwater flux, and (d) oceanic processes (advection + diffusion + entrainment). Heavy contours are the zero line.

are saltier than observed and saltier than the entrained water as there is not a large difference between salinity in and at the base of the mixed layer, which leads to negative entrainment. When entrainment is negative, it is not physically realistic and acts as a damping term toward climatology.

[37] To describe the salinity balance more synthetically, we determine the dominant process at each point in our domain by comparing the absolute value of the average of each term at each point grid. The resulting map of dominant terms is useful to summarize the salinity balance (Figure 11). In the northern tropical Atlantic, it shows that salinity variations are primarily controlled by the freshwater fluxes (strong precipitations due to the position of ITCZ) but advection and entrainment also contribute significantly. In the tropical south Atlantic, the advection term dominates, with freshwater flux (dominated by evaporation) and entrainment terms also contributing significantly. Also, we have to keep in mind that at each grid point, the dominant term is necessarily balanced by other terms, which can individually or collectively become dominant during part of the seasonal cycle (as we will see below).

3.4. Seasonal Variations

[38] The previous section focused on spatial variations of the annual mean MLS balance. Specific regions with high MLS variability due to typically different processes have been identified (Figure 2b). In this section, for each of these regions, we discuss the seasonal variations of the MLS balance. We first compare the seasonal cycle of the MLS tendency in the observations and in the model (Figure 12) and then rely on the model to examine how the various terms work during this seasonal cycle.

[39] The results for the western tropical Atlantic region (WTA; 7°–15°N, 45°–58°W) are presented in Figures 12a, 13a, and 13b. The model reproduces relatively well the seasonal evolution of the observed MLS (Figure 12a) and MLS tendency (Figure 13a). This is the region where the amplitude of the seasonal signal is maximum with a difference of more than 1.2 between maximum and minimum MLS. However, the modeled salinity is higher than observed and reaches its minimum in July, 1 month later than observed. The salinity tendency is negative from February–March to June, with the maximum decreasing trend in May, and

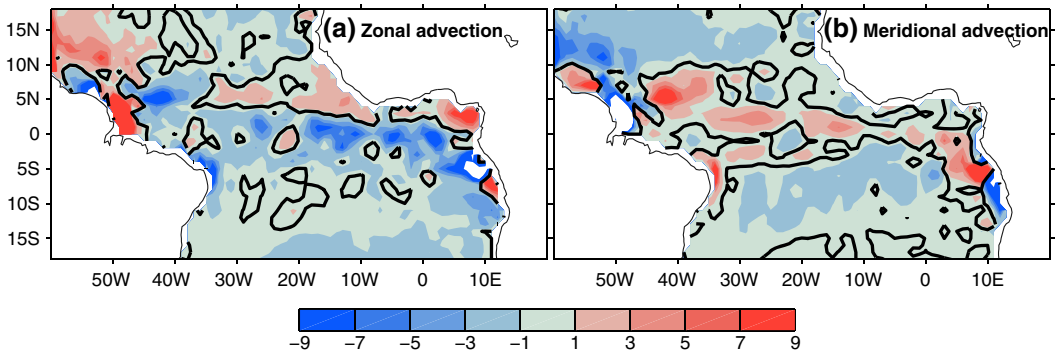

Figure 9. Annual mean for the (a) zonal and (b) meridional horizontal advection. Heavy contours are the zero line. Units are yr^{-1}.

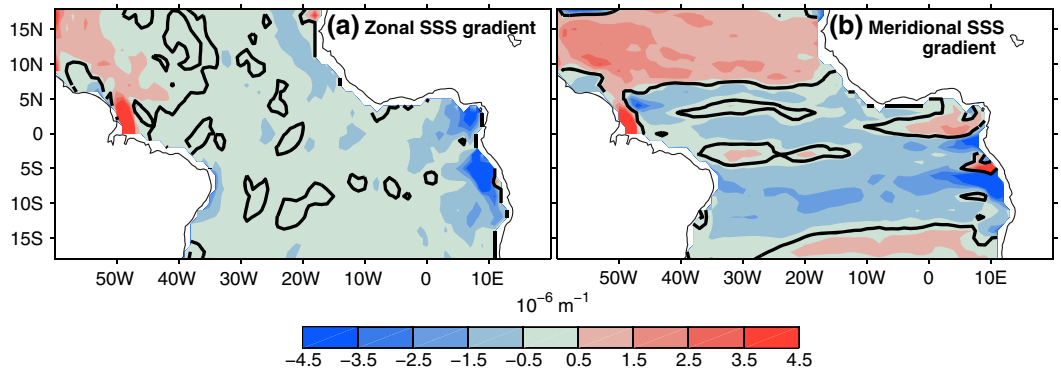

Figure 10. Annual mean for the (a) zonal and (b) meridional salinity gradient from the mixed layer salinity. Heavy contours are the zero line. Units are $10^{-6}\,m^{-1}$.

positive for the rest of the year. Then the MLS increases slowly for 8 months. The discrepancy between observed and modeled salinities could be due to an incorrect redistribution of the Amazon freshwaters as suggested earlier. These waters are advected to the north-west by the NBC from January to June (June being the month of the Amazon peak flow) [*Dai et al.*, 2009]. Then part of these waters is transported to the east in boreal summer and fall by the NECC [*Muller-Karger et al.*, 1988; *Dessier and Donguy*, 1994] when it reaches its maximum development [*Richardson and McKee*, 1984; *Bourlès et al.*, 1999]. Thus, the observed positive bias may be due to an overestimated transport of freshwaters by the NBC into the WTA box and the negative bias to an underestimated transport by the NECC out of the WTA box.

[40] For the salinity balance, we find that from March to November, the seasonal cycle of MLS is dominated by the horizontal advection terms (Figure 13b). The negative meridional advection dominates from March to June. This is due to northward transport by the NBC of Amazon freshwaters, with a maximum freshening effect in May roughly corresponding to the Amazon River discharge peak [*Dai et al.*, 2009]. In the rest of the year, zonal advection dominates and is mostly positive because currents are westward and zonal SSS gradient is positive. During December to February, the seasonal evolution of MLS is mainly controlled by the vertical entrainment and freshwater flux. These two terms create the peak of maximum salinity tendency term observed in December. The freshwater flux variations reflect the meridional displacement of the ITCZ: located south of this region most of the year, the ITCZ moves northward in boreal summer and reaches its northernmost position (just over this region) in September. This explains its tendency to decrease MLS from boreal summer to fall and to increase MLS during the rest of the year. The entrainment term is positive all year long as expected with the strong vertical stratification here due to fresh surface waters. Freshwater flux and entrainment terms tend to compensate each other from March to November. The diffusion term is negligible in this region.

[41] In the central tropical Atlantic (CTA (5°–15°N, 20°–45°W); Figure 12b), the modeled MLS slightly underestimates the observed field but the seasonal evolution is well reproduced and the simulated MLS tendency matches the observed seasonal evolution within error bars (Figure 13c). The salinity tendency is positive from November to April and negative for the rest of the year. It reaches a maximum in December and a minimum in September. These results are in agreement with *Foltz and McPhaden* [2008]. However, the salinity variations diagnosed by our model are closer to observations compared to those explicitly resolved in this previous study.

[42] Considering the contributions of the various terms of the salinity balance in the evolution of the seasonal cycle (Figure 13d), we find that the freshwater flux term dominates the seasonal cycle of MLS. It is in particular responsible for the peak of decreasing salinity tendency in September. This term is driven by the seasonal cycle of ITCZ activity, similarly to the WTA region (both regions located in the same latitude band). During the first half of the year, zonal and meridional advections are both weak and negative. During the rest of the year, they are of opposite sign and tend to compensate each other. Meridional advection shows a maximum freshening effect in May due to northward currents in the presence of a northward increasing SSS. The zonal advection dominates horizontal advection and shows a maximum freshening effect in boreal summer. This is due to eastward currents in the presence of a stronger positive zonal SSS gradient. The entrainment term is positive throughout the year. This term shows a seasonal cycle with a magnitude roughly similar to the horizontal advection term. This term always tends to bring salty water from below into the mixed layer. Its maximum effect occurs in December due to the maximum entrainment velocity in CTA region. Horizontal

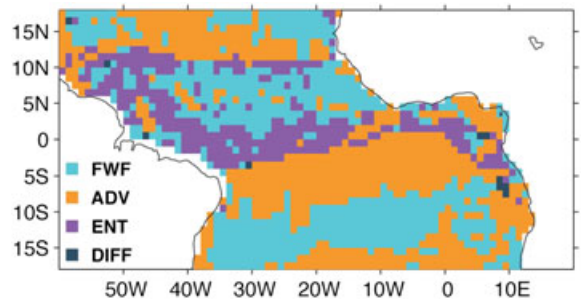

Figure 11. Map of the salinity dominant term in the tropical Atlantic Ocean: freshwater flux (FWF), horizontal advection (ADV), entrainment (ENT), and horizontal diffusion (DIFF).

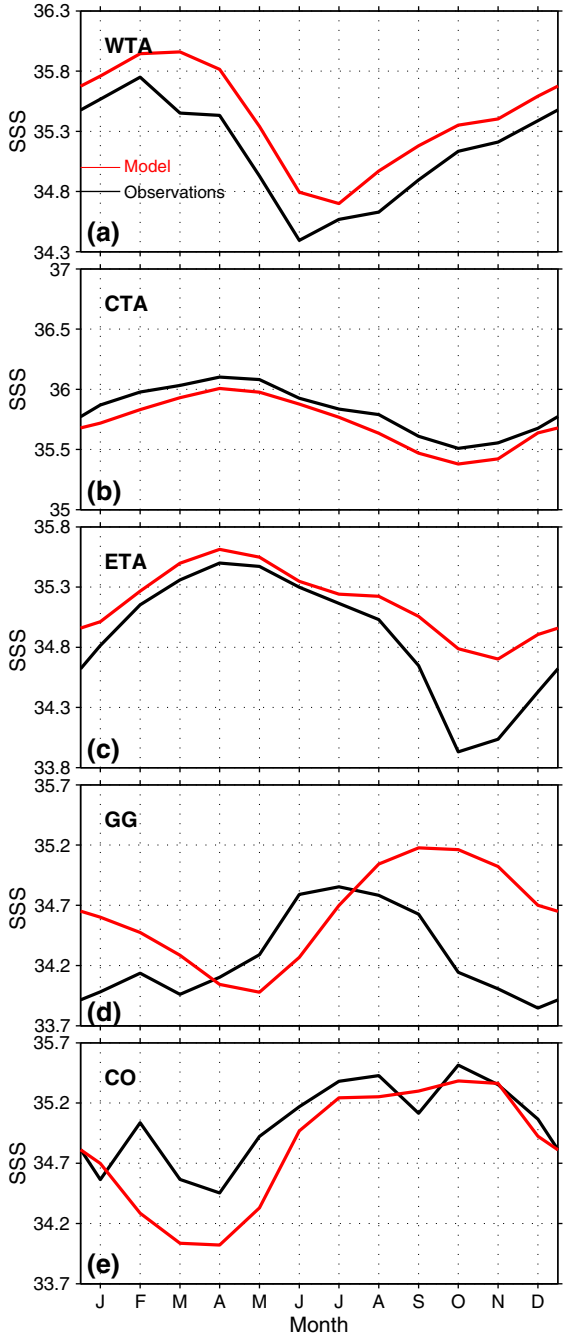

Figure 12. Seasonal cycle of mixed layer salinity from observation (in black) and from the model (in red) for the five selected regions (a) WTA, (b) CTA, (c) ETA, (d) GG, and (e) CO.

advection and entrainment processes almost compensate each other during the year. The diffusion term is once again negligible all year long. These results are mostly in agreement with the study by *Foltz and McPhaden* [2008] except that they did not explicitly compute the entrainment term. Our better match between model and observations confirms their suggestion on the key role of entrainment in this region.

[43] In the eastern tropical Atlantic (ETA (5°–15°N, 10°–20°W) region), from January to July, the seasonal evolutions of the observed and simulated SSS agree (Figure 12c). However, the modeled minimum SSS in October–November is less pronounced than observed. This can be explained by the sensitivity of the region to freshwater flux. We chose ERA-Interim precipitation product to force the model, but with NCEP2 precipitation product the amplitude of the seasonal signal in this region is better represented (not shown). Even though the seasonal signal in both precipitation products agrees, their amplitude is very different. The model reproduces quite well the observed evolution of the salinity tendency with only a small bias in July–August (Figure 13e). Between December and March, advection, entrainment, and freshwater flux equally contribute to the seasonal cycle of MLS (Figure 13f). During the rest of the year (April to November), freshwater flux and advection are the dominant terms. The freshwater flux is negative most of the year, except in boreal winter, which shows that it is dominated mainly by precipitation. This term has a seasonal cycle strongly driven by ITCZ variability, similarly to the WTA and CTA regions; its magnitude is greater than the advection terms. The entrainment term has a weak seasonal cycle and is positive throughout the year. Zonal advection (associated with the NECC) dominates over meridional advection, contrary to the WTA region, as alongshore currents are weaker at eastern (compared to western) oceanic boundaries. The zonal advection term is positive throughout the year as the eastward NECC brings waters saltier than coastal waters in this region.

[44] In the Gulf of Guinea (GG (2°S–5°N, 10°W–12°E) region), the model does not reproduce well the observed seasonal evolution of MLS nor its tendency (Figures 12d and 13g). The modeled seasonal cycle of MLS exhibits a 2 month lag for the observed seasonal minimum and maximum and it is amplified compared to observations (Figure 12d). The model underestimates the observed salinity tendency from November to May and overestimates the tendency for the rest of the year (Figure 13g). Also, the observed extrema (May maximum and October minimum) appear with a 2 month lag in the model. This is not surprising as this region combines a number of challenging issues. Coastal boundary conditions are crucial here, as this is the oceanic region that is most enclosed by land in our domain. However, the relatively poor resolution of the coastline, the introduction of the runoff coming out of the Niger delta in the model, and the neglect of secondary rivers are all critical points here. It is also a region where the mixed layer depth can be small and the model can thus be sensitive to changes in MLD. Also, we do not resolve vertical diffusion in the model; this is an important process for temperature in this region [*Jouanno et al.*, 2011a, 2011b], and it could be important for salinity too. The damping effect of the entrainment term, obviously strong near the Niger's mouth (Figure 8b), helps to offset these weaknesses but induces a delay which could also contribute to the lag between model and observations. Lastly, there are not many observations in this region (Figure 1), so even the climatology calculated with observations has significant uncertainties and does not allow us to firmly conclude on the accuracy of the simulated salinity tendency term.

[45] In the model, entrainment is the process with the strongest seasonal cycle (Figure 13h), due to the large difference between mixed layer salinity and subsurface salinity in this region. This term is the largest term from March to July,

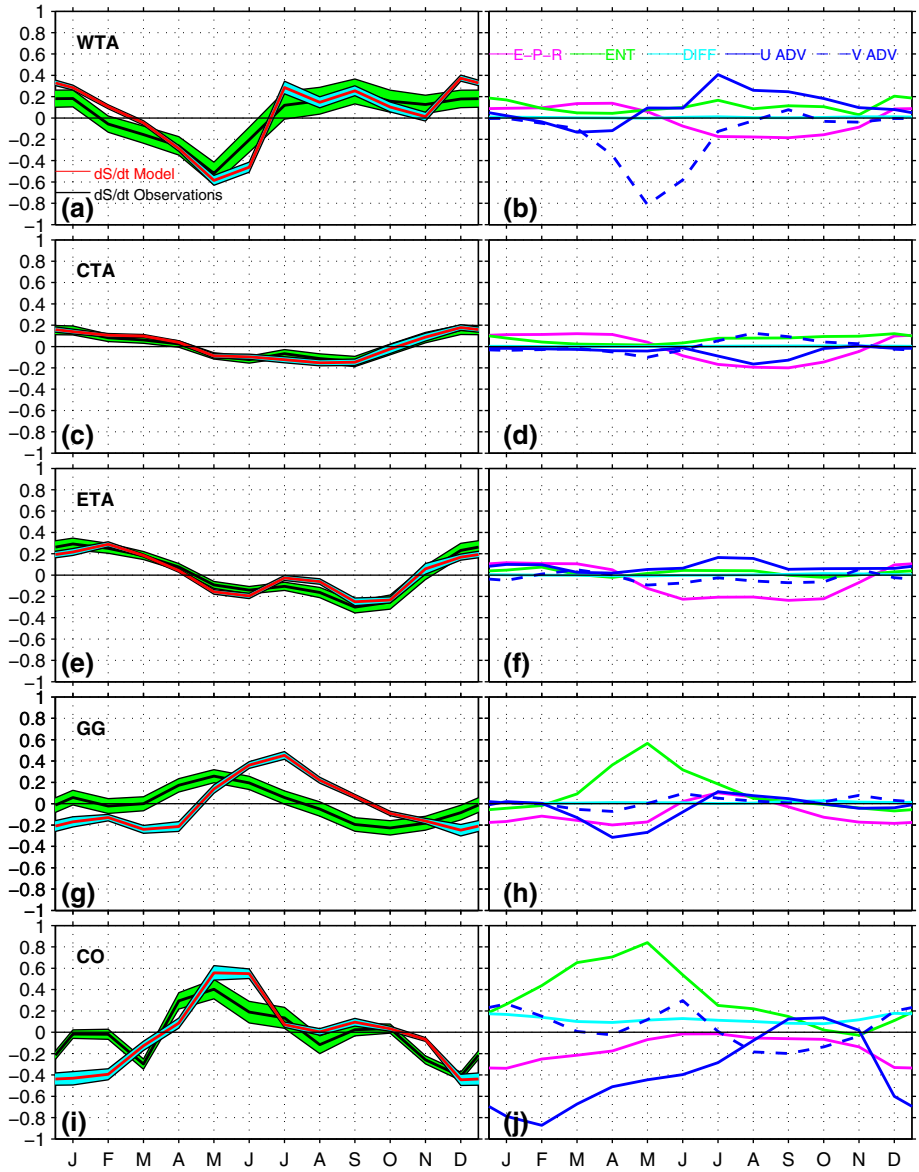

Figure 13. (a, c, e, g, and i) Salinity tendency terms in the mixed layer for each region with the shaded areas indicating error estimates (see Appendix A) for these two terms. (b, d, f, h, and j) Individual contributions to the salt balance equation of freshwater flux (purple), entrainment (green), horizontal diffusion (light blue), zonal advection (blue), and meridional advection (dashed blue). All terms in month^{-1}.

with a positive peak in May. However, from April to August, it strongly interacts with the advection and freshwater flux terms that are roughly in phase and negative before July. The positive entrainment peak in May is compensated by these processes. In July, these secondary terms become positive and add to the entrainment term, creating an annual peak in the MLS tendency. Between August and September, advection, entrainment, and freshwater flux equally contribute to the seasonal cycle of MLS. The rest of the year (October to February), the freshwater flux term drives the salinity balance. This term is negatively correlated with the freshwater flux term in the WTA, CTA, and ETA regions, as the GG region is located to the south of the mean latitude of the ITCZ.

[46] The mouth of Congo (CO (2°–8°S, 2°W–12°E) region) is under the direct influence of the Congo River that brings the second largest freshwater runoff to the ocean after the Amazon [*Dai et al.*, 2009]. The modeled and observed seasonal signals (Figure 12e) are in phase but the model overestimates the freshening of the surface waters at the minimum of the seasonal cycle. For the seasonal cycle of MLS tendency, both observations and model reach their maximum in May and their minimum in December (Figure 13i). Differences between modeled and observed MLS tendencies are small except at the beginning of the year (in January–March). However, this region has very sparse observational coverage and the uncertainty on the observed SSS product is high. This

is also true for the current product as indicated by *Lumpkin and Garzoli* [2005].

[47] In this region, Figure 13j shows that during September to December, the salinity tendency is driven by the freshwater flux as other terms roughly compensate each other. The freshwater flux is negative all year long, due to the strong input of freshwater from the river Congo (59%) as well as from precipitation (41%) in this region. This term reaches a peak in December due to the maximum Congo River discharge at that time of year. The horizontal advection term is strong and negative during most of the year. This is due to offshore advection by the westward SEC of fresh coastal waters. Horizontal advection is partly compensated by meridional advection that is negatively correlated with it. Overall, advection tends to drive the seasonal cycle of MLS from January to March. Then the entrainment term, with a positive peak in May, drives the salinity balance from April to August. Like in GG region, the maximum effect of the entrainment term in May is due to the large difference between mixed layer and subsurface salinity in this region. This region is the only one where the horizontal diffusion term is not negligible. It is slightly positive all year long, with a weak seasonal cycle.

4. Discussion and Conclusion

[48] This study attempts to diagnose the seasonal mixed-layer salinity (MLS) balance in the tropical Atlantic Ocean using a simplified model strongly constrained by observations, namely a combination of satellite products, atmospheric reanalyses, and monthly in situ observations. We take into account most terms affecting MLS: freshwater flux, horizontal advection, entrainment, and horizontal diffusion terms. Vertical diffusivity is not considered in this study. Thickness of the mixed layer is prescribed and is used to compute the entrainment term, which acts as a damping term for MLS and is important for the stability of the model.

[49] Observed SSS climatology products usually calculated through objective analysis or similar methods are rather uncertain in regions where observations are scarce, such as the eastern part of the Gulf of Guinea and Congo region. Except in these regions, our simulated mean state of SSS compares well with a climatology derived from observations.

[50] For the steady state, over the whole basin, the model indicates that all terms of salinity balance are important to describe the MLS. Sensitivity tests allowed us to select the most appropriate current product and freshwater flux. There are large uncertainties on E-P estimation in the tropics. Spatial patterns qualitatively agree, but differences in E-P range are important between the different products. There are also differences between currents products and the sensitivity tests suggest that MLS is more sensitive to currents than to freshwater flux in the model. Our sensitivity tests lead us to select ERA-Interim E-P and surface currents deduced from direct DRIFTER observations [*Lumpkin and Garzoli*, 2005] to optimize the model skills.

[51] The seasonal cycle of MLS was described using five regions of distinct characteristics to determine the evolution of the contribution of the various processes during its cycle. In the western tropical Atlantic (7°–15°N, 45°–58°W), from March to November the evolution cycle of MLS is dominated by the advection term. During the rest of the year, the advection term is weak and MLS variability is mainly controlled by freshwater flux and entrainment. In the central tropical Atlantic (5°–15°N, 20°–45°W), the seasonal cycle of MLS is mainly driven by the seasonal cycle of precipitation in this region. These results are consistent with *Foltz and McPhaden* [2008]. However, the salinity variations diagnosed by our model are closer to observations. The difference between the two studies lies in the entrainment term that they did not consider explicitly. This term appears to be important in this region. In the eastern tropical Atlantic (5°–15°N, 10°–20°W) from December to March, advection, entrainment and freshwater flux are equally important for describing MLS variability while during the rest of the year, the main drivers are freshwater flux and zonal advection. In the Gulf of Guinea (2°S–5°N, 10°W–12°E), salinity tendency is due to freshwater flux during October to February and to the entrainment and advection during March to July. The rest of the year (August to September) all terms are small. Finally, in the Congo region (2°–8°S, 2°W–12°E), the strong input of freshwater from the river Congo (59%) as well as from precipitation (41%) drives the variability of MLS from September to December. During January to March, MLS is driven by advection term. During the rest of the year (April to August), it is driven by vertical entrainment.

[52] The simulated salinity tendency terms capture reasonably well the observed seasonal cycle of MLS in all these regions. Model and observations present however some differences due in part to the limited observational coverage in some regions and to the model itself (because of its simplifying assumptions).

[53] In this study, the vertical physics is represented through the entrainment term. *Jouanno et al*. [2011a, 2011b] found that along the equator and in Gulf of Guinea the vertical diffusion is important for the temperature balance in the upper ocean. We argue that this term could also be important in MLS balance. So, to study the MLS balance in these regions, an Ocean General Circulation Model (OGCM) is probably necessary to correctly represent the vertical diffusion processes involved, to get the right balance of the near surface salinity. The inclusion of sophisticated vertical physics may lead to better performances than our model, in these regions. Another important point to mention is that the good performance of our model over most of the basin probably largely results from the prescribed subsurface salinity that prevents the simulated MLS to drift too far from observations. It will be interesting to assess the robustness of our conclusions in a model with both sophisticated vertical physics and prognostic salinity throughout the water column.

[54] There is an obvious lack of in situ SSS measurements in the eastern Gulf of Guinea. The recent launch of satellite missions dedicated to sea surface salinity measurement as Soil Moisture Ocean Salinity (SMOS) [*Reul et al*., 2012] and Aquarius [*Lagerloef*, 2012] offers the potential to quickly improve our knowledge of SSS, and therefore ocean dynamics, in such regions.

Appendix A: Error Estimates

[55] Sensitivity tests show in section 3.1 allow us to estimate the errors (ε_m) on model salinity tendency terms. We

run 16 model experiments with different combinations of ocean surface current and freshwater flux products. First, we calculate the model salinity tendency term for each simulation. Then, for each month of the seasonal cycle, standard error is estimated from all the simulations.

[56] For the observed mixed-layer salinity tendency, we first estimate SSS monthly errors (ε_S) as the standard error of all available observations in the 2000–2008 study period. Then, errors in mixed-layer salinity tendency (ε_{obs}) are estimated by using *Foltz and McPhaden*'s [2008] formula: $\varepsilon_{obs} = \left(\sqrt{\varepsilon_{S_{t+1}}^2 + \varepsilon_{S_{t-1}}^2}\right)/\Delta t$, with $\Delta t = 2$ months.

[57] **Acknowledgments.** We would like to thank Gilles Reverdin for his tremendous tenacity at collecting and validating available SSS observations to construct an update of Reverdin et al.'s 2007 product. A large part of the data comes from the French SSS observation service (http://www.legos.obs-mip.fr/observations/sss). C.Y. D-A would like to thanks the SCAC of the French Embassy in Cotonou, Bénin, and IRD for their support through PhD grants. Finally, sincere thanks are due to the reviewers, whose precious contributions helped to improve and complete the earlier versions of the paper.

References

Adler, R. F., et al. (2003), The Version 2 Global Precipitation Climatology Project (GPCP) monthly precipitation analysis (1979–present), *J. Hydrometeorol.*, *4*, 1147–1167.

Bretherton, F. P., R. E. Davis, and C. B. Fandry (1976), A technique for objective mapping and design of oceanographic experiments, *Deep Sea Res.*, *23*, 559–582.

Bonjean, F., and G. S. E. Lagerloef (2002), Diagnostic model and analysis of the surface currents in the tropical Pacific Ocean, *J. Phys. Oceanogr.*, *32*, 2938–2954.

Bourlès, B., Y. Gouriou, and R. Chuchla (1999), On the circulation in the upper layer in the western equatorial Atlantic, *J. Geophys. Res.*, *104*(C9), 21,151–21,170.

Bourlès, B., M. D'Orgeville, G. Eldin, Y. Gouriou, R. Chuchla, Y. du Penhoat, and S. Arnaul (2002), On the evolution of the thermocline and subthermocline eastward currents in the equatorial Atlantic. *Geophys. Res. Lett.*, 29.

Boyer, T. P., et al. (2009), World Ocean Database 2009. S. Levitus, Ed., NOAA Atlas NESDIS 66, U.S. Gov. Printing Office, Wash., D.C., 216 pp., DVDs.

Dai, A., T. Qian, K. Trenberth, and J. Milliman (2009), Changes in continental freshwater discharge from 1948 to 2004, *J. Clim.*, *22*, 2773–2792.

de Boyer Montégut, C. G. Madec, A. S. Fischer, A. Lazar, D. Ludicone (2004), Mixed layer depth over the global ocean: An examination of profile data and a profile-based climatology, *J. Geophys. Res.*, *109*(C12), 52–71.

de Boyer Montégut, C. J. Mignot, A. Lazar, and S. Cravatte (2007), Control of salinity on the mixed layer depth in the world ocean: Part 1: General description, *J. Geophys. Res.*, *107*, C06011, doi:10.1029/2006JC003953.

Dee, D. P., et al. (2011), The ERA-Interim reanalysis: Configuration and performance of the data assimilation system. *Q. J. R. Meteorol. Soc. 137*, 553–597, doi:10.1002/qj.828.

Delcroix, T., and C. Hénin (1991), Seasonal and interannual variations of sea surface salinity in the tropical Pacific Ocean, *J. Geophys. Res.*, *96*, 22,135–22,150.

Delcroix, T., M. J. McPhaden, A. Dessier, and Y. Gouriou (2005), Time and space scales for sea surface salinity in the tropical oceans, *Deep Sea Res., Part I*, *52*, 787–813.

Dessier, A., and J. R. Donguy (1994), The sea surface salinity in the tropical Atlantic between 10 S and 30 N seasonal and interannual variations (1977–1989), *Deep Sea Res., Part I*, *41*, 81–100.

Dong, S., S. L. Garzoli, and M. Baringer (2009), An assessment of the seasonal mixed layer salinity budget in the Southern Ocean, *J. Geophys. Res.*, *114*, C12001, doi:10.1029/2008JC005258.

Foltz, G. R., S. A. Grodsky, J. A. Carton, and M. J. McPhaden (2004), Seasonal salt budget of the northwestern tropical Atlantic Ocean along 38°W, *J. Geophys. Res.*, *109*, C03052, doi:10.1029/2003JC002111.

Foltz, G. R., and M. J. McPhaden (2008), Seasonal mixed layer salinity balance of the tropical North Atlantic Ocean, *J. Geophys. Res.*, *113*, C02013, doi:10.1029/2007JC004178.

Grodsky, S. A., R. Lumpkin, and J. A. Carton (2011), Spurious trends in global surface drifter currents, *Geophys. Res. Lett.*, *38*, L10606, doi:10.1029/2011GL047393.

Johnson, E. S., G. S. E. Lagerloef, J. T. Gunn, and F. Bonjean (2002), Surface salinity advection in the tropical oceans compared with atmospheric freshwater forcing: A trial balance, *J. Geophys. Res.*, *107*(C12), 8014, doi:10.1029/2001JC001122.

Johnson, E. S., F. Bonjean, G. S. E. Lagerloef, J. T. Gunn, and G. T. Mitchum (2007), Validation and error analysis of OSCAR sea surface currents, *J. Atmos. Oceanic Technol.*, *24*, 688–701.

Jouanno, J., F. Marin, Y. du Penhoat, J. M. Molines, and J. Sheinbaum, (2011a), Seasonal modes of surface cooling in the Gulf of Guinea, *J. Phys. Oceanogr.*, *41*, 1408–1416.

Jouanno, J., F. Marin, Y. du Penhoat, J. Sheinbaum, and J. M. Molines (2011b), Seasonal heat balance in the upper 100 m of the equatorial Atlantic Ocean, *J. Geophys. Res.*, *116*, C09003, doi:10.1029/2010JC006912.

Kanamitsu, M.,W. Ebisuzaki, J. Woollen, S. K. Yang, J. J. Hnilo, M. Fiorino, and G. L. Potter (2002), NCEP-DOE AMIP-II reanalysis (R-2), *Bull. Am. Meteorol. Soc.*, *83*, 1631–1643.

Kawabe, M. (2008), Vertical and horizontal eddy diffusivities and oxygen dissipation rate in the subtropical northwest Pacific, *Deep Sea Res., Part I*, *55*, 247–260, doi:10.1016/j.dsr.2007.12.003.

Lagerloef, G. S. E. (2002), Introduction to the special section: The role of surface salinity on upper ocean dynamics, air-sea interaction and climate, *J. Geophys. Res.*, *107*(C12), 8000.

Lagerloef, G. S. E., G. T. Mitchum, R. B. Lukas, and P. P. Niiler (1999), Tropical Pacific near-surface currents estimated from altimeter, wind, and drifter data, *J. Geophys. Res.*, *104*(C10), 23,313–23,326.

Lumpkin, R., and S. L. Garzoli (2005), Near-surface circulation in the tropical Atlantic Ocean, *Deep Sea Res., Part I*, *52*, 495–518.

Lagerloef, G. S. E. (2012), Satellite mission monitor ocean surface salinity. *E.O.S., 93*, *25*(23), 4233–234.

Lukas, R., and E. Lindstrom (1991), The mixed layer of the western equatorial Pacific Ocean, *J. Geophys. Res.*, *96*(suppl), 3343–3357.

Mignot, J., C. de Boyer Montegut, A. Lazar, and S. Cravatte (2007), Control of salinity on the mixed layer depth in the world ocean: 2. Tropical areas, *J. Geophys. Res.*, *112*, C10010, doi:10.1029/2006JC003954.

Millero, F. J. (1993), What is PSU?, *Oceanogr.*, *6*(3):67.

Muller-Karger, F. E., C. R. McClain, and P. L. Richardson (1988), The dispersal of the Amazon's water, *Nature*, *333*, 56–58.

Pailler, K., B. Bourlès, and Y. Gouriou (1999), The barrier layer in the western tropical Atlantic Ocean, *Geophys. Res. Lett.*, *26*, 2069–2072.

Rao, R. R., and R. Sivakumar (2003), Seasonal variability of sea surface salinity and salt budget of the mixed layer of the north Indian Ocean, *J. Geophys. Res.*, *108*(C1), 3009, doi:10.1029/2001JC000907.

Reul, N., J. Tenerelli, J. Boutin, B. Chapron, F. Paul, E. Brion, F. Gaillard, and O. Archer (2012), Overview of the first SMOS sea surface salinity products, *IEEE Trans. Geosci. Remote Sens.*, *50*(5), 1636–1647, doi:10.1109/TGRS.2012.21884081.

Reverdin, G., E. Kestenare, C. Frankignoul, and T. Delcroix (2007), Surface salinity in the Atlantic Ocean (30°S–50°N), *Prog. Oceanogr.*, *73*, 311–340, doi:10.1016/j.pocean.2006.11.004.

Richardson, P. L., and T. K. McKee (1984), Average seasonal variation of the Atlantic equatorial currents from historical ship drifts, *J. Phys. Oceanogr.*, *14*, 1226–1238.

Sprintall, J., and M. Tomczak (1992), Evidence of the barrier layer in the surface layer of the tropics, *J. Geophys. Res.*, *97*, 7305–7316.

Sudre J., and R. A. Morrow (2008), Global surface currents: A high-resolution product for investigating ocean dynamics, *Ocean Dyn.*, *58*, 101–118, doi:10.1007/s10236-008-0134-9.

Taylor, K. (2001), Summarizing multiple aspects of model performances in a single diagram, *J. Geophys. Res.*, *106*(D7), 7183–7192.

Xie, P. P., and P. A. Arkin (1997), Global precipitation: A 17-year monthly analysis based on gauge observations, satellite estimates, and numerical model outputs, *Bull. Am. Meteorol. Soc.*, *78*, 2539–2558.

Yu, L., X. Jin, and R. Weller (2008), Multidecade global flux datasets from the Objectively Analyzed air-sea Fluxes (OAFlux) Project: Latent and sensible heat fluxes, ocean evaporation, and related surface meteorological variables, 64 pp.

Yu, L. (2011), A global relationship between the ocean water cycle and near surface salinity, *J. Geophys. Res.*, *116*, C10025, doi:10.1029/2010JC006937.